Journal of Applied Polymer Science

Influences of Processing on the Phase Transition and Crystallization of Polypropylene Cast Films

Meng Xu,[1,2] Shijun Zhang,[2] Jieying Liang,[1] Hui Quan,[2] Jianye Liu,[2] Hongwei Shi,[2] Dali Gao,[2] Jie Liu[1]

[1]Key Laboratory of the Ministry of Education on Carbon Fibers and Functional Polymer, Beijing University of Chemical Technology, Beijing 100029, China

[2]Beijing Research Institute of Chemical Industry, SINOPEC, Beijing 100013, China

Correspondence to: J. Liu (E-mail: liuj@mail.buct.edu.cn)

ABSTRACT: Phase transition and changes of properties of isotactic polypropylene (i-PP) cast films with the processing conditions have been investigated by wide-angle X-ray diffraction, two-dimensional small-angle X-ray scattering, and atomic force microscopy. It was found that chill roll temperature was a major factor, which influenced the formation of mesomorphic phase and its transition to spherulitic structure. Only mesomorphic phase was observed in the films produced under a chill roll temperature of below 40°C. When the roll temperature was increased to 60°C, mesomorphic phase coexisted with spherulitic crystal structure, and totally transformed to monoclinic structure at the roll temperature of 80°C. Differential scanning calorimetry, tensile, and optical tests were also performed on the films. The results showed that the observed structure changes were closely related to the thermal behavior, tensile, and optical properties of the PP films. The influence of die temperature on the films was also discussed, but the effect was much less than chill roll temperature. © 2014 Wiley Periodicals, Inc. J. Appl. Polym. Sci. **2014**, *131*, 41100.

KEYWORDS: crystallization; films; morphology; phase behavior; polypropylene

Received 24 March 2014; accepted 31 May 2014

DOI: 10.1002/app.41100

INTRODUCTION

Isotactic polypropylene (i-PP) is a kind of important commercial thermoplastic material, which has been widely used in various applications. i-PP has three kinds of crystal structures (α-,β-, and γ-form) depending on crystallization conditions.[1–4] The fourth polymorph of i-PP is an intermediate state between amorphous and crystalline phase, and so-called "mesomorphic phase."[5–7] The mesomorphic phase of i-PP contains a 3_1 helical conformation similar to the helix in the crystallization of α-form, and the structure of the mesomorphic phase is confirmed by infrared spectroscopy,[8] wide-angle X-ray scattering (WAXS)[9–11] and small-angle X-ray scattering (SAXS).[12,13] The mesomorphic phase can often be obtained by quenching the molten polymer at a drastic rate of over 100°C/s, and the quenching can be performed using differential scanning calorimetry (DSC) or fast scanning chip calorimetry.[14–19] The formation of mesomorphic phase will be inhibited when the target temperature is lower than the glass transition and the cooling rate is faster than 1000°C/s.[20,21] Mesomorphic phase can be also obtained by cold-drawing. Tensile deformation-induced mesomorphic phase have been widely studied as processing extensively influenced the structure and properties of i-PP.[22–24] The differences of structure and morphology between quench-induced mesomorphic phase and deformation-induced mesomorphic phase have also been investigated by SAXS and WAXS.[25]

The morphology of mesomorphic phase can be evaluated by atomic force microscopy (AFM) or transmission electron microscopy (TEM),[26,27] and is described as a granular domains so-called "nodule." The size of the nodular domains differs slightly with the quenching conditions and properties of i-PP. An 0.25-mm-thick PP film manufactured using melt-extrusion on a cooling roll of 18°C has a nodule size of 10 nm, while i-PP films quenched from melt into ice water or ethanol/dry ice mixture contain nodular domains of 10–20-nm size.[21,28]

Mesomorphic phase can be transformed into crystalline phase by annealing the quenched i-PP. The annealing process is often carried out using fan-assisted oven,[29] DSC[19,30] or hot stage of situ-AFM,[30] situ-wide-angle X-ray diffraction (WAXD),[31] and situ-SAXS.[26] The DSC scanning often shows a small endothermic peak from 40 to 80°C on the heating curves, indicating the mesomorphic phase reorganizing and converting into crystalline phase.[11,25] However, the transformation, which is detected by WAXD or SAXS, happens lately at the temperature above

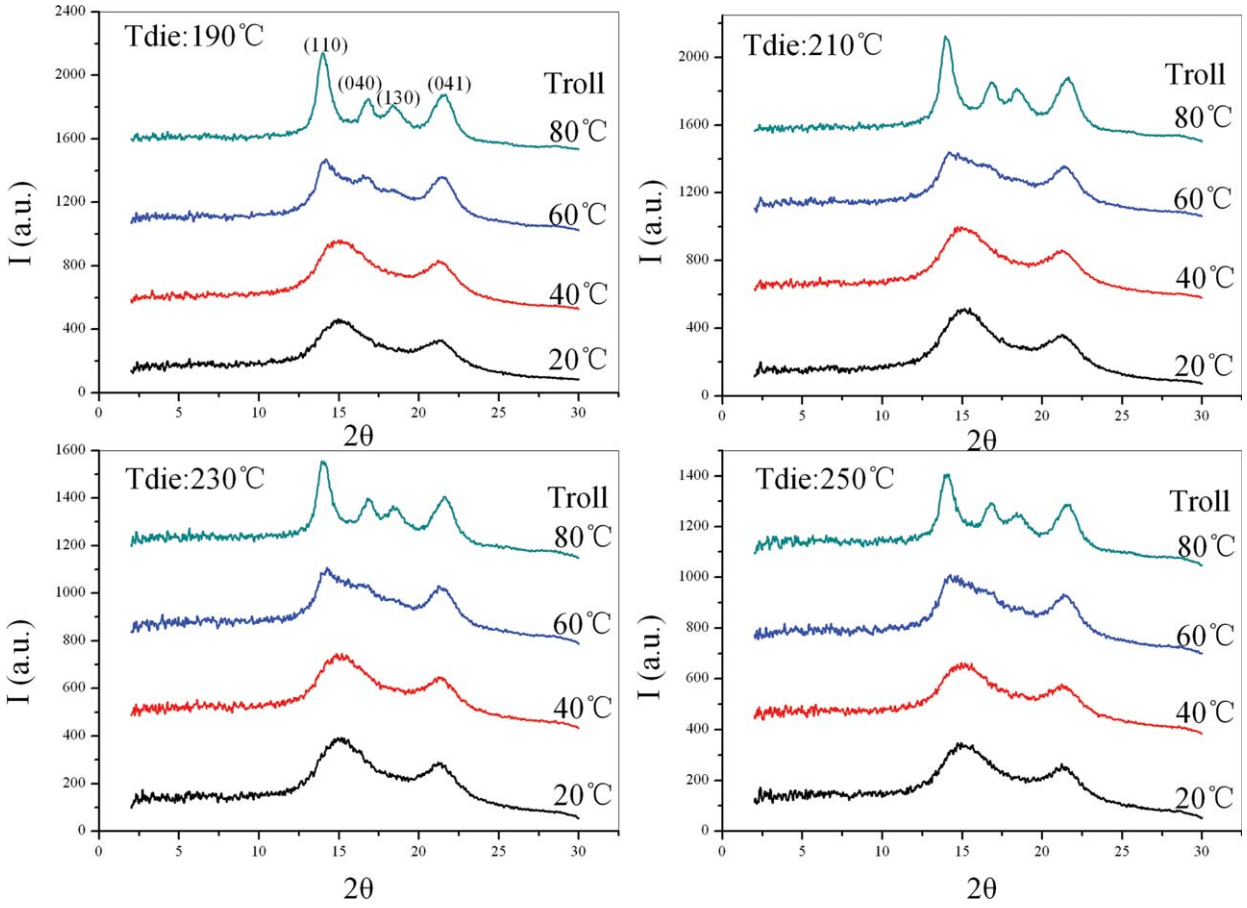

Figure 1. WAXD profiles of PP films prepared under different chill roll temperatures and die temperatures. [Color figure can be viewed in the online issue, which is available at wileyonlinelibrary.com.]

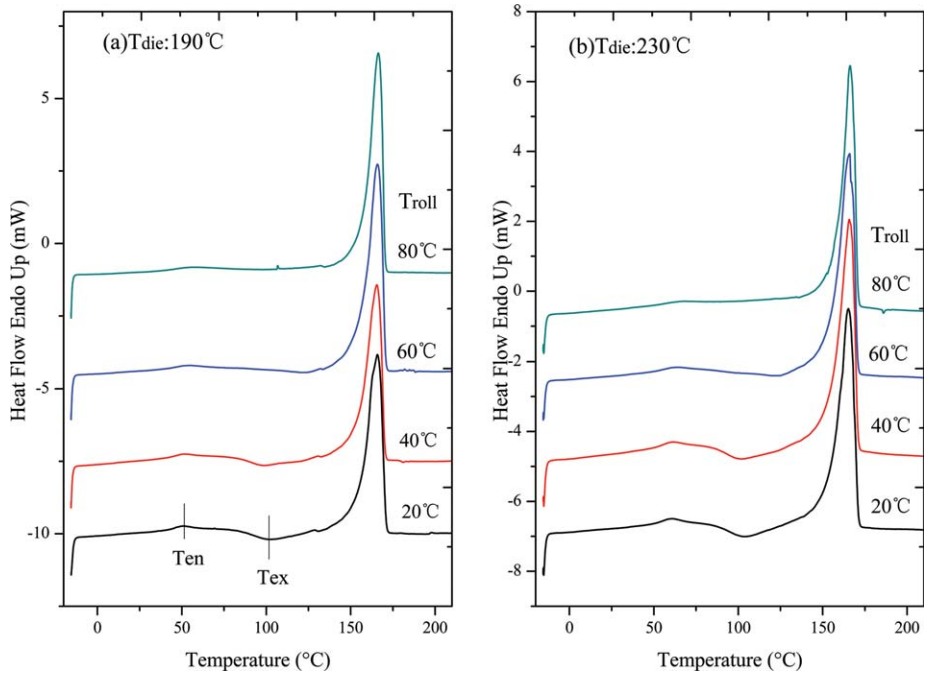

Figure 2. DSC melting curves of PP films prepared under different chill roll temperatures and die temperatures, obtained at 10°C/min. [Color figure can be viewed in the online issue, which is available at wileyonlinelibrary.com.]

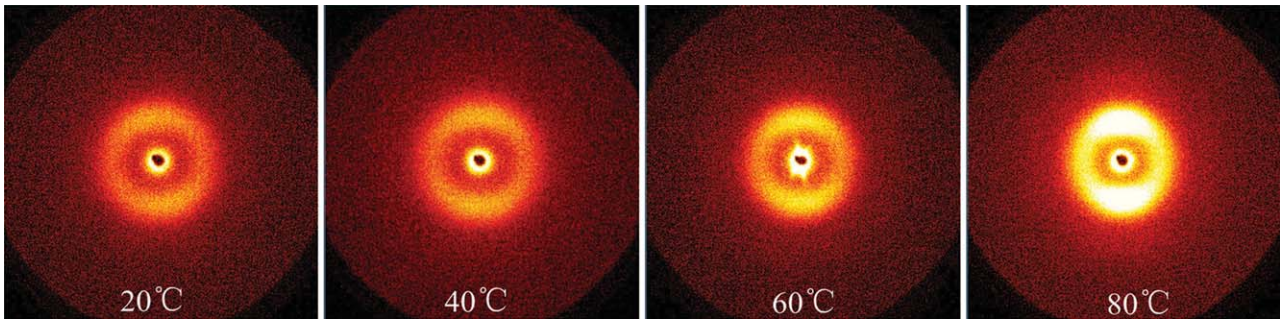

Figure 3. 2D-SAXS patterns of films for chill roll temperatures of 20°C, 40°C, 60°C, and 80°C; $T_{die} = 190$°C; MD ↑ and TD →. [Color figure can be viewed in the online issue, which is available at wileyonlinelibrary.com.]

70–80°C. Wang et al.[32] attributed this to the low quantity of α-form crystals, which could not be revealed by the X-ray measurements.

Several studies have focused on the effect of processing conditions or further treatment on the structure of PP films.[29,33–36] The change and relationships of structure, surface morphology, and properties of biaxially oriented films or blown films are also widely discussed.[37,38] But as we known, fewer researches are about the cast-extruded processing,[39] and rare research is about the influence of chill roll temperature. In these studies, the temperature of chill roll is set as low as possible so the films can be rapidly cooled.[26,29,34] Tabatabaei et al.[40] investigated cooling condition in cast film process, but their main results were obtained under the chill roll temperature above 100°C. In our study, we conducted the cast film process under different chill roll temperatures (20–80°C) and die temperatures (190–250°C). We described the phase transition under these different temperatures based on the results of WAXD, two-dimensional small-angle X-ray scattering (2D-SAXS), AFM, and DSC. The effect of phase transition on the thermal behavior, mechanical, and optical properties of PP films was also discussed in detail.

EXPERIMENTAL

In this study, a Ziegler-Nata isotactic polypropylene (i-PP) was investigated, which was synthesized by Beijing Research Institute of Chemical Industry with a melt flow rate of 7.0 g/10min (at 230°C, 2.16 kg). Its number- and weight-averaged molecular weight was 59,000 and 303,000 g/mol, respectively, according to gel permeation chromatography (GPC) results. As measured by DSC at a heating/cooling rate of 10°C/min, the melting point (T_m) and crystallization temperature (T_c) of the i-PP resin was 165.9 and 122.3°C, respectively.

The i-PP material was cast-extruded using a cast film line from Labtech Engineering Company to obtain films with a thickness of about 30 μm. The line was equipped with a 2-mm thick and 350-mm width slit die and two chill rolls. The air-gap between the die and the first chill roll was 10 mm. The temperature of screw extruder was 230°C and the die temperatures were set at 190, 210, 230, and 250°C, respectively. An air knife closed to the die was used to supply low-flow-rate air to the film surface. The air knife had a 3-mm-thick and 350-mm-width slit, and the air flow rate was 1 m/s. For all the die temperatures, the chill roll temperatures were set as 20, 40, 60, and 80°C. Prior to measurement, the films were conditioned at 23°C, 50% RH for 48 h to obtain a stable structure.

WAXD experiments were carried out on the D8 DISCOVER 2D X-ray diffractometer. The X-ray was generated using IμS micro Focus X-ray source incorporating a 50 W generator sealed-tube X-ray generator with Cu target. The wavelength is 0.1542 nm. The power of the generator used for measurement was 50 kV and 1 mA. The X-ray intensities were recorded on a VÅNTEC-500 2D detector system with a pixel size of 68 × 68 μm^2. The distance from the sample to detector was 91 mm. The spot size of the beam was 0.5 mm. The exposure time was 180 s. The original experimental data such as data acquisition and background subtraction were handled by GADDS software. The films were cut into small samples and hold with a fixture especially designed for films for investigation.

SAXS experiments were conducted using Bruker NANOSTAR U SAXS instrument equipped with a Hi Star two-dimensional detector. The X-ray source is IμS-type generator and operated at 40 kV and 650 mA resulting in a wavelength (l) of 1.54 Å (CuKα) in the experiment. The detector-to-sample distance is 1053 mm resulting a resolvable range of 0.10 nm$^{-1} \leq q \leq$ 2.0 nm^{-1}, where q is scattering vector ($q = 4\pi/\lambda \sin\theta$, $2q$ is scattering angle). The 3-pinhole collimation system provides a precisely parallel X-ray beam with high intensity. The scattering intensity was detected by the Hi Star area detector with 1024 × 1024 pixels and 100 mm pixel size. To get enough scattering intensity, several layers of films were stacked to obtain a total thickness of about 2 mm.

The morphology on the surface of films was obtained using Vecco NanoScopeIIIa AFM instrument with a NanoProve SPM

Table I. Identification and Characteristic Values of PP Films Under Investigation, Obtained from DSC

T_{die} (°C)	T_{roll} (°C)	T_{en} (°C)	T_{ex} (°C)	T_m (°C)
190	20	51.4	101.9	165.8
190	40	52.1	99.0	165.4
190	60	54.5	123.5	165.9
190	80	56.0	-	166.4
230	20	61.2	103.9	165.2
230	40	61.5	101.9	165.0
230	60	64.7	124.7	165.4
230	80	66.0	-	165.6

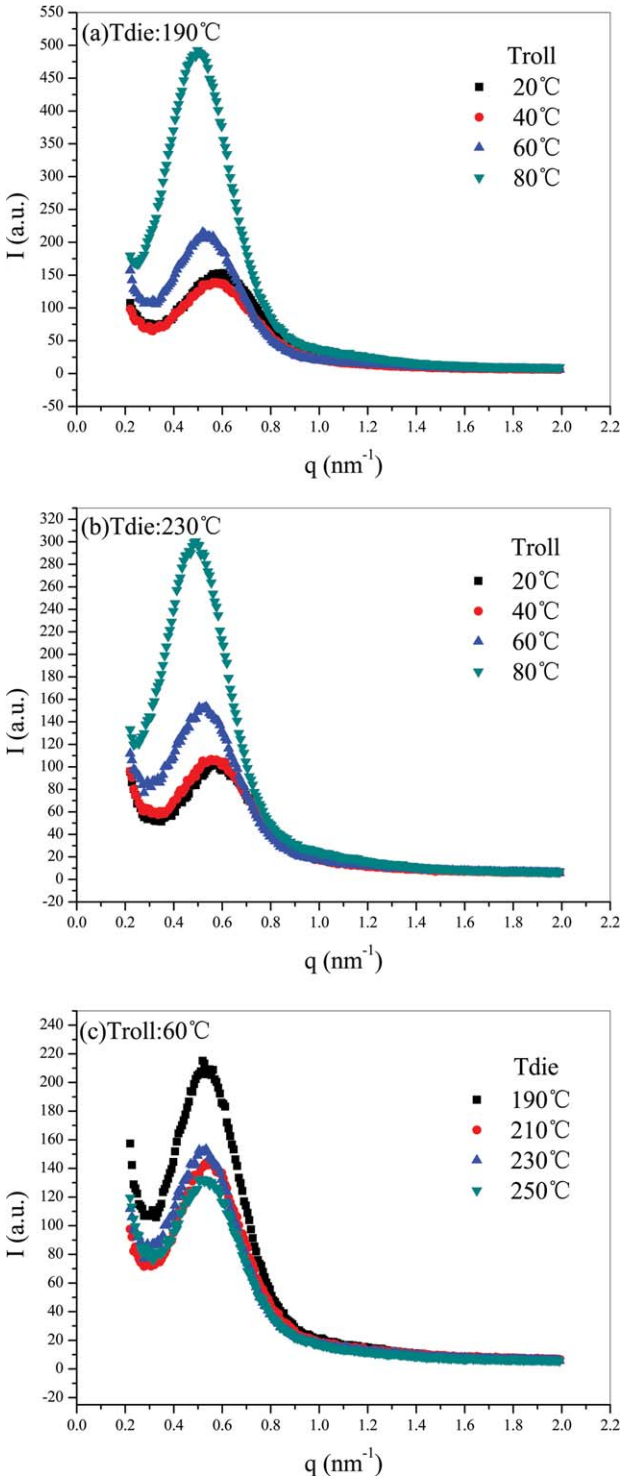

Figure 4. SAXS intensity profiles for films prepared under different chill roll temperatures and die temperatures. [Color figure can be viewed in the online issue, which is available at wileyonlinelibrary.com.]

Si probe with a cantilever length of 125 μm and an elasticity coefficient of 42 N/m. AFM was performed in tapping mode (frequency: 300 KHz) to get the height imaging. The films were cut into small samples (the surface, which attached to the chill roll, was put upward) and fixed on a metallic holder for investigation.

A Perkin-Elmer Diamond thermal analysis system was used to study the thermal properties of the film samples. The films were cut to fragments, and about 5 mg samples were put into aluminum pans and sealed. The samples were heated from −10 to 220°C at 10°C/min. The nitrogen gas flow was 30 mL/min.

Tensile tests were performed using an Instron 5500 universal testing instrument with a 100 N load cell. The films were cut into rectangular specimen and tested according to ASTM D638-03 at a crosshead speed of 500 mm/min. Gloss of films was analyzed using a BYK gloss testing instrument based on the standard ASTM D2457-08.

RESULTS AND DISCUSSION

Figure 1 shows WAXD grams of films prepared under different die temperatures (T_{die}) and chill roll temperatures (T_{roll}). All the WAXD profiles under different T_{die} show the same trend with the change of T_{roll}. When T_{roll} are 20 and 40°C, there are two broad peaks at $2\theta = 15.0°$ and 21.4°, which are considered to be attributed to the mesomorphic phase. The first peak is considered as the average interchain distance, and the second refers to the 3_1 helical conformation.[24] When T_{roll} rises to 80°C, the two broad mesomorphic phase reflections split into the (110), (040), (130), and (141) reflections of the monoclinic crystals and the WAXD profiles at T_{roll} of 60°C show an intermediate trend between the curves of mesomorphic phase and crystalline phase.

The DSC results represented in Figure 2 shows that thermal behavior of films is also affected by T_{roll} and T_{die}. When T_{roll} is lower than 60°C, three transition peaks can be seen on the DSC curves, a broad endotherm peak (T_{en}), exothermic peak (T_{ex}), and the main melting peak (T_m) at about 166°C. The data of all the transition peaks are listed in detail in Table I. As has already been stated by other studies,[24,25,40] the first endotherm peak around 51–66°C related to the melting process of the mesomorphic phase and small crystals, and the exotherm is referred to a reordering process of the melted mesomorphic phase and small

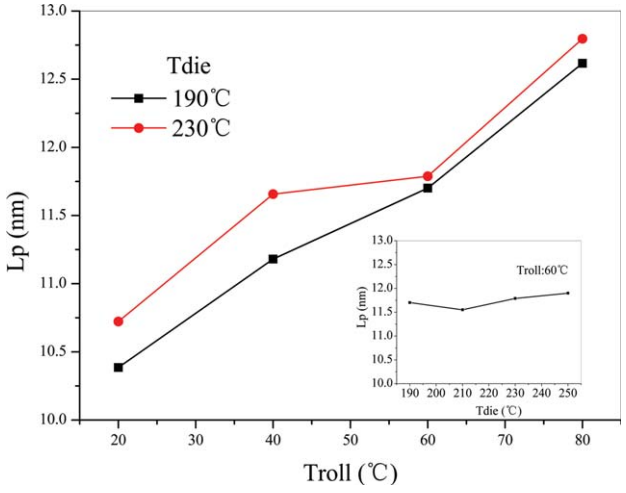

Figure 5. Evolution of the long period distance with chill roll temperatures and die temperatures. [Color figure can be viewed in the online issue, which is available at wileyonlinelibrary.com.]

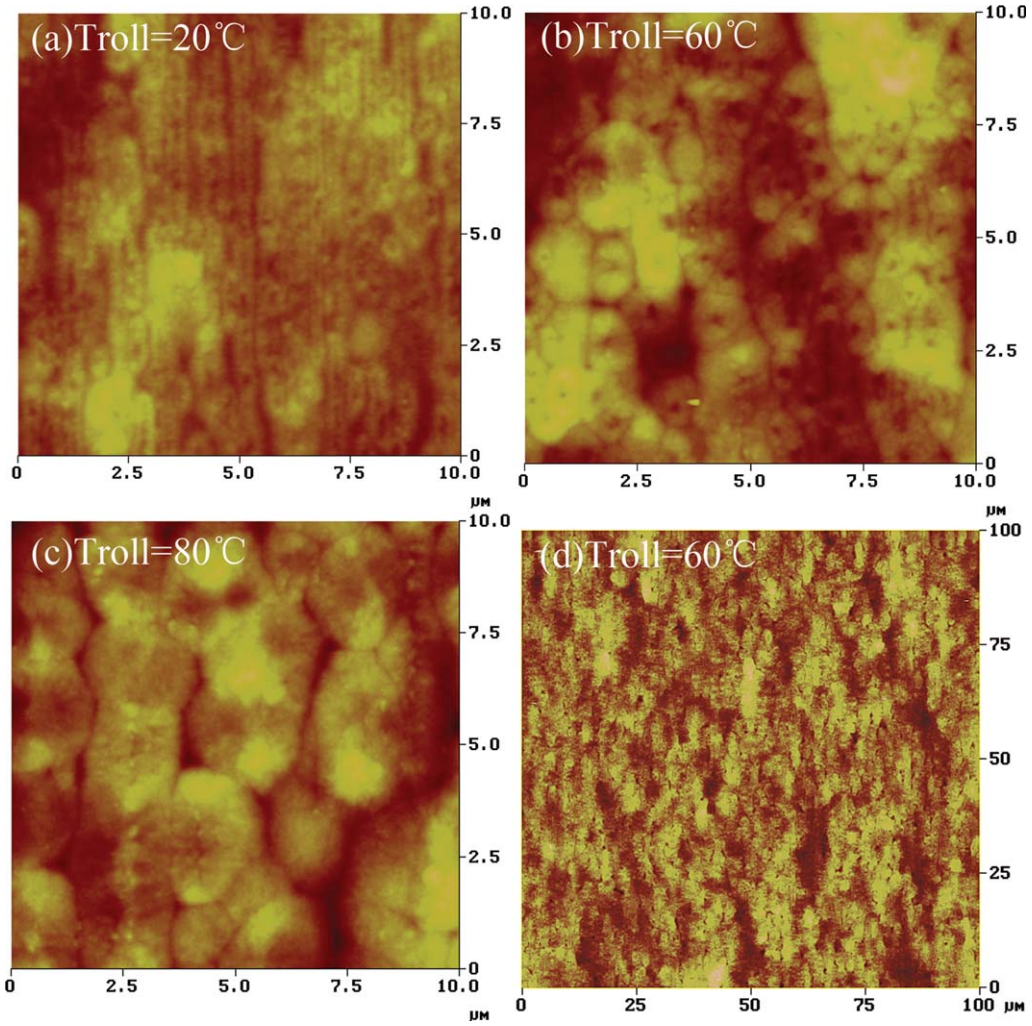

Figure 6. AFM images of the surface of the films obtained at different chill roll temperatures; $T_{die} = 190°C$; MD ↑ and TD →. [Color figure can be viewed in the online issue, which is available at wileyonlinelibrary.com.]

crystals to form a more stable monoclinic crystal structure. The exothermic peak cannot be observed anymore for T_{roll} of 80°C. This can be explained by the WAXD result that mesomorphic phase is not contained in the films prepared under the highest T_{roll}. As a result, the weak exotherm related to the reordering processes of mesomorphic phase totally disappears on DSC curves.

From Table I, we can see that the peak position of exotherm is near 100°C for T_{roll} of 20 and 40°C, and goes up to a much higher temperature range (above 120°C) for T_{roll} of 60°C. WAXD patterns show that mesomorphic phase and monoclinic structure are coexisting in the films manufactured under higher T_{roll}, For the monoclinic does not melt at the temperature range of the first endotherm, we suppose that the monoclinic structure restrain the molecular chain mobility of mesomorphic and amorphous phase, which cause the reordering process happen at a higher temperature.

In biaxial or uniaxial drawing process, orientation often plays an important role in the structure and properties of films.[25] We also studied the orientation of the films using the 2D-SAXS. The SAXS patterns of films under different chill roll temperatures at T_{die} of 190°C are shown in Figure 3. The pictures of samples under T_{die} of 230°C are not represented for they have similar patterns as Figure 3. The 2D-SAXS patterns present an isotropic diffuse scattering ring of T_{roll} below 40°C, then display a weak orientation along machine direction (MD) at T_{roll} of 60°C, and finally transform to elliptical pattern, which indicates a higher orientation when T_{roll} rises to 80°C. However, the orientation is so weak that it cannot induce a mesomorphic phase structure. It also does not have an important influence on the mechanical properties of the films, which will be discussed afterward. It can be also seen that the scattering intensity of the films increases with the T_{roll}, especially increases dramatically at T_{roll} of 80°C. The enhancement of the scattering intensity implies higher amount of ordered microstructures along MD is inclined to form under higher T_{roll}.

Figure 4 illustrates the meridional SAXS intensity profiles of the films at different T_{roll} and T_{die}. Because the samples are all composed of several layers of PP film, the scale of intensity cannot be accurately obtained, but the change trend of intensity can be

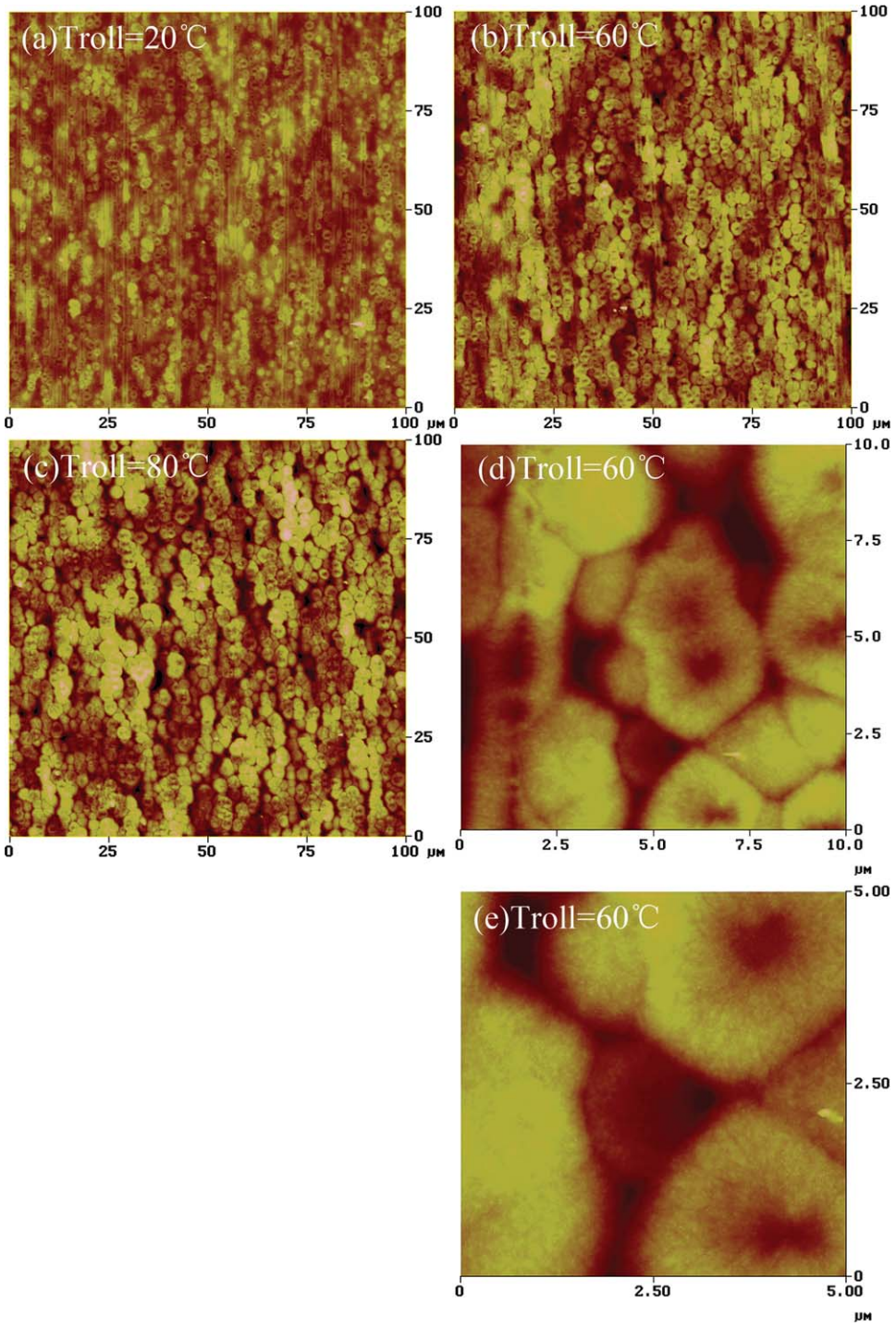

Figure 7. AFM images of the surface of the films obtained at different chill roll temperatures; $T_{die} = 230°C$; MD ↑ and TD →. [Color figure can be viewed in the online issue, which is available at wileyonlinelibrary.com.]

clearly seen. The intensity peak shifts to lower position, being accompanied with the increase of peak intensity as T_{roll} increases. However, the influence of T_{die} on the peak position is not so obvious.

The scattering vector q ($q = 4\pi/\lambda \sin \theta$) and the peak position of q with the maximum intensity (q_m) are also demonstrated. The long period distance (Lp) is calculated by the Bragg's law, $Lp = 2\pi/q_m$, and the relationship of Lp and processing conditions is represented in Figure 5. When T_{roll} increases from 20 to 80°C, the value of Lp increases from 10.4 to 12.6 nm at T_{die} of 190°C, and from 10.7 to 12.8 nm at T_{die} of 230°C. T_{die} does not have a big influence on the value of Lp. Sadeghi et al.[33] found that, the long space was about 10 nm for mesomorphic phase in cast PP film, which corresponded to a cluster structure

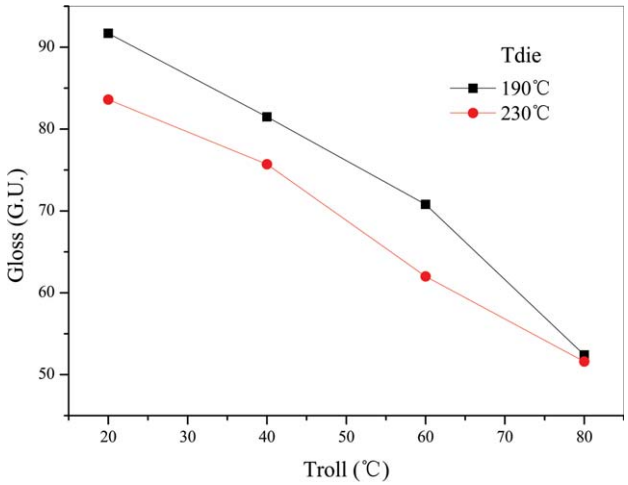

Figure 8. Gloss of the individual films prepared under T_{die} of 190°C and 230°C in dependence of T_{roll}. [Color figure can be viewed in the online issue, which is available at wileyonlinelibrary.com.]

having the adjacent spacing observed by TEM. This result is in agreement with the Lp of our films manufactured under T_{roll} of 20°C. Combining with the WAXD, the increasing Lp along with the temperature can be explained either by larger mesomorphic structure or higher content of crystalline structure.

As the previous results implied, significant differences in the crystal structure and size of films under different chill roll temperatures can be clearly visualized from AFM images (Figures 6 and 7). All the AFM images are based on the side attached to the chill roll, which is much smoother and propitious to represent the effect of chill roll on the morphology of the film. Figure 6 shows the height images of films manufactured under T_{die} of 190°C. As Figure 6(d) presented, high variation of films under this T_{die} is slight, so larger scan size of 10 × 10 μm^2 is performed in Figure 6(a–c). When T_{roll} is 20°C, a large amount of stripe structures orientating along MD can be observed in Figure 6(a). The stripe structures are almost replaced by spherical structures of diffuse size at T_{roll} of 60°C [Figure 6(b)], which grow up and turn to more uniform and bigger spherical crystal structures at T_{roll} of 80°C, as demonstrated in Figure 6(c).

AFM images of the films manufactured under T_{die} of 230°C are presented in Figure 7. The films prepared under this die temperature all show a larger surface height variation, so their morphologies can be observed clearly at a scan size of 100 × 100 μm^2. Along with the increasing chill roll temperature, the films at T_{die} of 230°C have the same phase transition process as the change shown in Figure 6. Corresponding to the SAXS results, higher die temperature and chill roll temperature can increase the size of microstructures in the films. The size change can also affect the thermal behavior, which is shown in Table I. The peak position of the first endotherm increases with roll temperature, and T_{en} of samples under the same T_{roll} increases about 10°C while T_{die} grow up from 190 to 230°C. Cooling at higher temperature seems to lead structures in bigger size, which need more energy to be melt and reorganized.

Based on the results of WAXD and SAXS, the stripe structure observed in AFM images at the lowest T_{roll} can be considered as a symbol of mesomorphic phase. Though small crystals also exist, they cannot be detected by WAXD or SAXS due to their low amount and size. For T_{roll} of 60°C, the stripe structure can be hardly observed in AFM images, but the previous WAXD results still indicated the mesomorphic phase and monoclinic structure were coexisting in the films. From the finer surface structure of the film represented in Figure 7(d,e), we can see a small spherical structure coexists with complete spherical crystal under this T_{roll}. So we may suppose that the small spherical structure observed in AFM images for T_{roll} of 60°C is another symbol of mesomorphic phase, but have a different morphology and size.

From Figures 6(a) and 7(a), we can see the stripe structure orientate along MD, but this orientation is not shown in Figure 3(a). Previous studies found that the mesomorphic phase was composed of nodular domains having a size of about 10 nm.[27,28,30] Although an orientation can be observed at a relatively larger scale, the nodules may still disordered at a

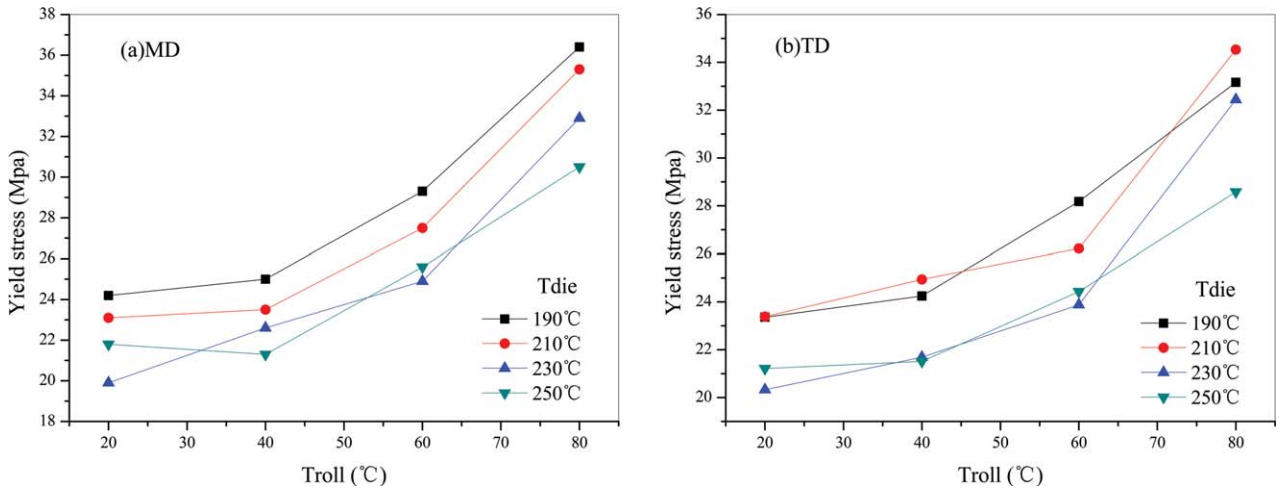

Figure 9. Dependence of the yield strength of the films prepared under different T_{die} on chill roll temperature. [Color figure can be viewed in the online issue, which is available at wileyonlinelibrary.com.]

nanoscale. By contrast, the partly ordered crystalline structure presented in other images of Figures 6 and 7 is in agreement with the 2D-SAXS patterns. The possible cause may be that the lamellae structure contained in the spherical crystals is partly ordered along MD.

Die temperature has an influence on the surface height variation of the films, which also affects the gloss of films. Slighter surface height change refers to a smoother surface of the films under T_{die} of 190°C, which is supported by Figures 6 and 8. The gloss of the films decreases rapidly with the increasing chill roll temperature. This can be explained by the increasing amount and size of spherical crystal structure in the films. When T_{roll} is 80°C, gloss of films under all the die temperatures is close to each other, for all the films contain spherulite structures of the same average size at this T_{roll}.

The corresponding mechanical properties of all the samples are represented in Figure 9. We can see the yield strength of PP films along MD and transverse direction (TD) grow rapidly above T_{roll} of 40°C. The mechanical properties are influenced strongly by the structure of films. When T_{roll} was below 40°C, considerable amount of mesomorphic structures are existing in the films. Qiu et al.[25] suggested that when tensile was performed on the films mainly containing mesomorphic phase, the mesomorphic phase would be induced to rotate accompanying partial elongation of the amorphous domains before yielding point, so the yield strength was decided by the deformation of mesomorphic phase and amorphous structure. However, as the amount and size of spherulitic structures increase with the enhancing T_{roll}, the yield strength strongly increase due to much more demanded energy consumption to break such structure. Our results are in good agreement with Ferrer-Balas et al.[41] who claimed that the tensile properties were highly improved during the transition of sm-PP (mesomorphic phase) to α-PP. We can also see in Figure 9 that MD and TD yield strength of same sample only have slight difference. This is in keeping with the SAXS results that the MD orientation is too small to generate an extensive variance between the two directions. Therefore, orientation is not the major factor for the films produced by cast-extrusion.

Based on the results above, we can also explain the effect of chill roll and die temperatures on the microstructure of the films in two ways. First, as mesomorphic phase can be induced by the process of quenching PP melt rapidly, the cooling of PP melt on the chill roll is similar to the quenching process, and the T_{roll} and T_{die} can affect the cooling rate. Higher cooling rate (lower T_{roll} and T_{die}) is conducive to freeze the molecular chains at a mesomorphic phase. Reversely, lower cooling rate (higher T_{roll} and T_{die}) is inclined to leave adequate time for the chains to form monoclinic structure. In the other aspect, the chill roll may play the role either in cooling the melt or in annealing the films. According to the DSC results, the width of first endotherm is from 40 to 80°C, which coincides with some of the chill roll temperatures we performed. We also know that T_{die} is not a major factor to affect the structure, so we can suppose that all the PP samples had a similar structure before attaching the chill roll. Moreover, as the films have a thickness of 20–30 μm, we suppose that the cooling is uniform and efficiency. So when the chill roll temperature is below 40°C, the formed mesomorphic phase is stable. On the contrary, all the mesomorphic phase will melt and reform a monoclinic structure at T_{roll} of 80°C and when the chill roll is in the endotherm range, only part of the mesomorphic phase vanish. Considering the energy brought by PP melt, the actual temperature range may be lower than the endotherm range obtained by DSC.

CONCLUSIONS

In summary, we have investigated the structures and properties of PP cast films produced under different chill roll temperatures and die temperatures. We find that the temperatures, especially the chill roll temperature, have crucial effects on the structure of PP cast films. Films produced under lower chill roll temperature contain small crystals and mesomorphic phase, which has a tripe shape observed by AFM. The proportion of monoclinic crystal increases along with chill roll temperature. Increasing long period distance and spherical structures of bigger size are observed either. Only slight orientation along MD is detected by SAXS for all the films, so orientation is not an important factor in cast film process. The influence of die temperature is not as obvious as chill roll temperature, but it seems lower temperature can lead to smoother surface for the films. We postulate that chill roll below 40°C can quench the melt rapidly and induce the formation of mesomorphic phase. However, when chill roll temperature is above 60°C, the chill roll cannot freeze the motion of molecular chains immediately, but provide limited amount of energy for part of the molecular chains to form monoclinic but not mesomorphic phase. At last, films with complete spherulitic crystal structure are produced by a chill roll at a high enough temperature of 80°C. Increasing chill roll temperature also causes great enhancement of yield stress and decrease of gloss, due to higher content and size of spherulitic crystal structure under higher chill roll temperature.

REFERENCES

1. Natta, G.; Corradini, P. *Nuovo Cimento Suppl.* **1960**, *15*, 40.
2. Addink, E. J.; Beintema, J. *Polymer* **1961**, *2*, 185.
3. Turner-Jones, A.; Aizlewood, J. M.; Beckett, D. R. *Makromol. Chem.* **1964**, *75*, 134.
4. Mancik, Z. *J. Macromol. Sci. Phys.* **1972**, *36*, 101.
5. Hsu, C. C.; Geil, P. H.; Miyaji, H.; Asai, K. *J. Polym. Sci. Part B: Polym. Phys.* **1986**, *24*, 2379.
6. Natta, G.; Peraldo, M.; Corradini, P. *Rend. Accad. Naz. Lincei* **1959**, *26*, 14.
7. Natta, G. *Makromol. Chem.* **1960**, *35*, 94.
8. Miller, R. L. *Polymer* **1960**, *1*, 135.
9. McAllister, P. B.; Carter, T. J.; Hinde, R. M. *J. Polym. Sci. Polym. Phys. Ed.* **1978**, *16*, 49.
10. Mileva, D.; Zia, Q.; Androsch, R.; Radusch, H.-J.;Piccarolo, S. *Polymer* **2009**, *50*, 5482.
11. Wang, Z. G.; Hsiao, B. S.; Srinivas, S.; Brown, G. M.; Tsou, A. H.; Chen, S. Z. D.; Stein, R. S. *Polymer* **2001**, *42*, 7561.

12. Miyamoto, Y.; Fukao, K.; Yoshida, T.; Tsurutani, N.; Miyaji, H. *J. Phys. Soc. Jpn.* **2000**, *69*, 1735.
13. Minami, S.; Tsurutani, N.; Miyaji, H.; Fukao, K.; Miyamoto, Y. *Polymer* **2004**, *45*, 1429.
14. Wu, Z. Q.; Dann, B. L.; Cheng, S. Z. D.; Wunderlich, B. *J. Thermal Anal.* **1988**, *34*, 105.
15. Zia, Q.; Androsch, R.; Tadusch, H.-J.; Piccarolo, S. *Polymer* **2006**, *47*, 8163.
16. Zia, Q.; Mileva, D.; Androsch, R. *Macromolecules* **2008**, *41*, 8095.
17. Androsch, T. *Macromolecules* **2008**, *41*, 553.
18. Mileva, D.; Androsch, R.; Zhuraviev, E.; Schick, C. *Macromolecules* **2009**, *42*, 7275.
19. Androsh, R.; Di Lorenzo, M. L.; Schick, C.; Wunderlich, B. *Polymer* **2010**, *51*, 4639.
20. Caldas, B.; Brown, G. R.; Nohr, R. S.; MacDonald, J. G.; Raboin, L. E. *Polymer* **1994**, *35*, 899.
21. Miyamoto, Y.; Fukao, K.; Yoshida, T.; Tsurutani, N.; Miyaji, H. *J. Phys. Soc. Jpn.* **2000**, *69*, 1735.
22. Ran, S.; Zong, X.; Fang, D.; Hsiao, B. S.; Chu, B.; Phillips, R. A. *Macromolecules* **2001**, *34*, 2569.
23. Ran, S.; Zong, X.; Fang, D.; Hsiao, B. S.; Chu, B.; Cunniff, P. M. *J. Mater. Sci.* **2001**, *36*, 3071.
24. Saraf, R. P. *Polymer* **1994**, *35*, 1359.
25. Qiu, J.; Wang, Z. G.; Yang, l.; Zhao, J. C.; Niu, Y. H.; Hsiao, B. S. *Polymer* **2007**, *48*, 6934.
26. Zia, Q.; Androsch, R.; Radusch, H. J.; Ingolic, E. *Polym. Bull.* **2008**, *60*, 791.
27. Androsch, R. *Macromolecules* **2008**, *41*, 533.
28. Grubb, D. T.; Yoon, D. Y. *Polym. Commun.* **1986**, *27*, 84.
29. Resch, K.; Wallner, G.; Teichert, C.; Maier, G.; Gahleitner, M. *Polym. Eng. Sci.* **2006**, *46*, 520.
30. Cao, J.; Sbarski, I. *Polymer* **2006**, *47*, 27.
31. Konishi, T.; Nishida, K.; Kanaya, T. *Macromolecules* **2006**, *39*, 8035.
32. Wang, Z.G.; Hsiao, B.S.; Sirota, E.B.; Agarwal, P.; Srinivas, S. *Macromolecules* **2000**, *33*, 978.
33. Sadeghi, F.; Ajji, A.; Carreau, P. *J. Polym. Eng. Sci.* **2007**, *47*, 1170.
34. Lin, Y.J.; Dias, P.; Chen, H.Y.; Hiltner, A.; Baer, E. *Polymer* **2008**, *49*, 2578.
35. Dias, P.; Lin, Y. J.; Hiltner, A.; Baer, E.; Chen, H. Y.; Chum, S. P. *J. Appl. Polym. Sci.* **2008**, *107*, 1730.
36. Aniunoh, K.; Harrison, G. M. *Polym. Eng. Sci.* **2010**, *50*, 1151.
37. Phillips, R. A.; Nguyen, T. *J. Appl. Polym. Sci.* **2001**, *80*, 2400.
38. Tamura, S.; Ohta, K.; Kanai, T. *J. Appl. Polym. Sci.* **2012**, *124*, 2725.
39. Lamberti, G.; Brucato, V.; Titomanlio, G. *J. Appl. Polym. Sci.* **2002**, *84*, 1981.
40. Tabatabaei, S. H.; Carreau, P. J.; Ajji, A. *Polymer* **2009**, *50*, 4228.
41. Ferrer-Balas, D.; Maspoch, M. L.; Martinez, A. B.; Santana, O.O. *Polymer* **2001**, *42*, 1697.